

Calculation of light scattering of an elliptical Gaussian beam by a spherical particle

JIANQI SHEN,*  XIANG LIU, WEI WANG, AND HAITAO YU

University of Shanghai for Science and Technology, Shanghai 200093, China

*Corresponding author: jqshen@163.com

Received 28 February 2018; revised 18 June 2018; accepted 18 June 2018; posted 18 June 2018 (Doc. ID 325122); published 9 July 2018

The use of an elliptical Gaussian beam (EGB) for applications relying on light scattering depends much on the ability to evaluate the beam shape coefficients (BSC) effectively and accurately. Based on the angular spectrum decomposition (ASD) of the radial components of the beam field, we present the formulations of the BSCs for the EGB. Numerical calculations of the BSCs, the beam reconstruction, and light scattering are performed. The fidelity of the reconstructed field to the given one is discussed so as to examine the BSC calculation. A comparison of the ASD method with the quadrature and localized approximation methods leads to the conclusion that the ASD method is much faster than the quadrature method, and it is very powerful for acquiring reliable and accurate results of BSCs, even for far off-axis locations and high ellipticities of the EGB. © 2018 Optical Society of America

OCIS codes: (290.4020) Mie theory; (290.5850) Scattering, particles; (140.3295) Laser beam characterization; (300.6300) Spectroscopy, Fourier transforms.

<https://doi.org/10.1364/JOSAA.35.001288>

1. INTRODUCTION

Most laser diodes or solid-state lasers emit elliptical Gaussian beams (EGB). Besides, the EGB can also be obtained by focusing a circular Gaussian beam (CGB) with a cylindrical lens or by refracting a CGB at obliquely incident angles. EGBs have been used in various measurement techniques relying on light scattering, such as optical particle sizing, particle image velocimetry, particle hologram, optical trapping, and manipulation [1–6].

Light scattering by a spherical particle requires a description of the incident beam in the spherical coordinate system, whose origin is fixed at the center of the particle. The incident beam field is expanded into an infinite series of spherical vector wave functions (SVWFs), each of which is weighted by an expansion coefficient. These coefficients are called beam shape coefficients (BSC). The use of EGB for applications relying on light scattering depends much on the ability to evaluate efficiently and accurately the BSCs that describe the beam profile. In the past few decades, different methods have been developed that can be classified into direct and indirect methods. The generalized Lorenz–Mie theory (GLMT) is one of the direct methods, in which a physical description of the beam in terms of radial electrical and magnetic field components E_r and H_r is required for evaluating the BSCs [7]. Another direct method utilizes the whole beam field \mathbf{E} or \mathbf{H} [8]. The angular spectrum decomposition (ASD) method is an indirect method, in which the electromagnetic field is modeled as a superposition of

monochromatic plane waves traveling in different directions [9–11], and each plane wave is expanded into SVWFs.

One of the issues in the BSC calculation is the efficiency of numerical computation. For this purpose, different methods have been developed in the GLMT, including the quadratures, the infinite series, the localized approximation (LA), and the integral LA (ILA) [12–16]. The quadrature methods appear under two formulations, one using three-dimensional integrals over all the three spherical coordinates r , θ , and ϕ , and the other using two-dimensional integrals over the polar angle θ and the azimuth angle ϕ . The latter is much faster than the former because it requires one less integration. The quadrature methods are very time consuming because the functions to be integrated oscillate greatly, which limits their applications. The LA and ILA methods relied on an analogy to van de Hulst's localization principle [17]. As a result, the integration over the polar angle is avoided, which speeds up the BSC calculation greatly. The ASD method uses two-dimensional integrals over the polar and azimuth angles in the Fourier space. This method is more efficient than the double quadrature of the GLMT, because functions to be integrated in ASD are not as oscillatory as those in GLMT. Another trial to improve the efficiency of numerical computation is to separate the azimuth-dependent terms from the beam field and carry out the azimuth integration analytically. This simplifies the BSC calculation into one-dimensional integration, which is ten times faster than the two-dimensional integrations. An example of this for a CGB can be found in Ref. [18].

Another issue in the BSC calculation is the accuracy of results, which can be examined by the fidelity of the reconstructed beam to the given one. Since the EGB can only be given in its low-order approximations, the beam field does not satisfy Maxwell's equations rigorously. However, its SVWF expansion is a strict solution to Maxwell's equations. Therefore, remodeling must occur in the methods for BSC evaluation, which determines the deviation of the reconstructed beam from the original one. The fidelity of the reconstructed beam to the given one reveals the remodeling of the methods for BSC calculation. Besides, the accuracy of BSC results also depends closely on the power of the numerical method that is employed in the BSC calculation, i.e., the ability of the method for getting reliable results for various beam parameters.

In the past, scattering of the CGB has been studied extensively, but for the EGB, as far as we know, there are only limited publications (e.g., Refs. [16,19–21]) due to the similarity of the beam profiles. However, since the CGB is only a special case of the EGB, light scattering of an EGB is noteworthy. The BSC calculation of an EGB is much more difficult than that of the CGB. In some cases, incorrect results of the BSCs may be obtained due to the loss of significant digits in numerical computation [22], which will be further discussed later in this paper.

The work aims at light scattering of an EGB by a spherical particle. In order to reveal the difference of remodeling in the quadrature method of GLMT and in the ASD method, expressions of BSCs are derived by expanding the radial components of the electric and magnetic fields of the EGB into the angular spectra. The BSCs in the quadrature and ASD methods are expressed in terms of one-dimensional integrals. The efficiency and accuracy of the methods are discussed by analyzing the BSC results and the corresponding reconstructed beam fields. Examples of the scattered light intensities are given.

2. ANALYTICAL FORMULATIONS

A. General Description of the Fields

In processing light scattering of a spherical particle, multiple expansion of the beam field in terms of SVWFs is required. The SVWFs have the following form:

$$\begin{cases} \tilde{\mathbf{M}}_{nm}^{(i)} = \frac{Z_n^{(i)}(\rho)}{\rho} e^{im\phi} [im\tilde{\pi}_n^m(\theta)\mathbf{e}_\theta - \tilde{\tau}_n^m(\theta)\mathbf{e}_\phi] \\ \tilde{\mathbf{N}}_{nm}^{(i)} = \frac{Z_n^{(i)}(\rho)}{\rho^2} e^{im\phi} n(n+1)\tilde{P}_n^m(\theta)\mathbf{e}_r \\ \quad + \frac{Z_n^{(i)'}(\rho)}{\rho} e^{im\phi} [\tilde{\tau}_n^m(\theta)\mathbf{e}_\theta + im\tilde{\pi}_n^m(\theta)\mathbf{e}_\phi] \end{cases}, \quad (1)$$

where (r, θ, ϕ) are the radius, polar, and azimuth angles in the spherical coordinate system (as shown in Fig. 1); \mathbf{e}_r , \mathbf{e}_θ , and \mathbf{e}_ϕ are the unit vectors, respectively; $Z_n^{(i)}(\rho)$ represents the Riccati–Bessel functions, where $i = 1$ for the incident beam and the field inside the particle and $i = 3$ for the scattering field; $\rho = kr$ is the dimensionless radial, wherein k is the wave-number; and $\tilde{P}_n^m(\cos \theta)$ is the normalized associated Legendre

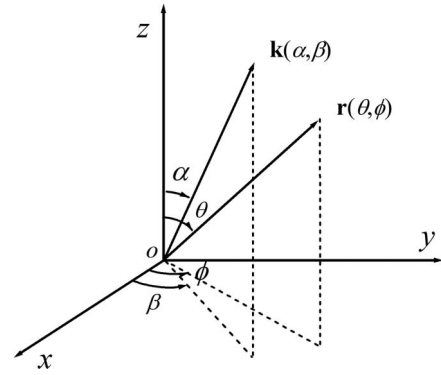


Fig. 1. Geometrical scheme of the coordinates.

function (NALF) of degree n and order m . Following Ferrer's definition, it is given as

$$\tilde{P}_n^m(x) = \sqrt{\frac{(2n+1)(n-m)!}{2(n+m)!}} (1-x^2)^{\frac{m}{2}} \frac{1}{2^n n!} \frac{d^{m+n}}{dx^{m+n}} (x^2-1)^n, \quad (2)$$

where $x = \cos \theta$. $\tilde{\pi}_n^m(\theta)$ and $\tilde{\tau}_n^m(\theta)$ are the generalized Legendre functions (GLFs) defined as $\tilde{\pi}_n^m(\theta) = \tilde{P}_n^m(\theta)/\sin \theta$ and $\tilde{\tau}_n^m(\theta) = d\tilde{P}_n^m(\theta)/d\theta$; the negative time convention $\exp(-i\omega t)$ is omitted, where ω is the angular frequency of light.

The electromagnetic field of the incident beam is expanded into

$$\begin{cases} \mathbf{E}^{\text{inc}} = E_0 \sum_{n=1}^{\infty} \sum_{m=-n}^n c_n^{pw} \{iA_{nm}\tilde{\mathbf{N}}_{nm}^{(1)} - B_{nm}\tilde{\mathbf{M}}_{nm}^{(1)}\} \\ \mathbf{H}^{\text{inc}} = H_0 \sum_{n=1}^{\infty} \sum_{m=-n}^n c_n^{pw} \{A_{nm}\tilde{\mathbf{M}}_{nm}^{(1)} + iB_{nm}\tilde{\mathbf{N}}_{nm}^{(1)}\} \end{cases}. \quad (3)$$

The BSCs A_{nm} and B_{nm} , following Barton's notation [23], describe the characteristics of the incident beam. The factor $c_n^{pw} = i^n(2n+1)/2n(n+1)$ also appears in the expansion of a plane wave (the superscript pw stands for plane wave). E_0 and H_0 are the amplitudes of the electric and magnetic fields at a chosen position (usually the beam center), satisfying the relation $E_0 = \sqrt{\mu/\epsilon}H_0$, where ϵ and μ are, respectively, the permittivity and permeability of the medium. If the beam field to be expanded is an exact solution to Maxwell's equations, the BSCs describe the given beam exactly [8]. In contrast, if the given beam does not satisfy Maxwell's equations rigorously, the determination of the BSCs produces a remodeling of the beam, which depends on the way it occurs. In this case, the SVWF expansion at the right hand side of Eq. (3) gives an approximation of the incident beam.

As long as the BSCs have been determined, the internal field and the scattered field can be described with

$$\begin{cases} \mathbf{E}^{\text{int}} = E_0 \sum_{n=1}^{\infty} \sum_{m=-n}^n c_n^{pw} \{id_n A_{nm}\tilde{\mathbf{N}}_{nm}^{(1)} - c_n B_{nm}\tilde{\mathbf{M}}_{nm}^{(1)}\} \\ \mathbf{H}^{\text{int}} = H_0 \sum_{n=1}^{\infty} \sum_{m=-n}^n c_n^{pw} \{d_n A_{nm}\tilde{\mathbf{M}}_{nm}^{(1)} + ic_n B_{nm}\tilde{\mathbf{N}}_{nm}^{(1)}\} \end{cases}, \quad (4)$$

$$\begin{cases} \mathbf{E}^{\text{sca}} = -E_0 \sum_{n=1}^{\infty} \sum_{m=-n}^n c_n^{pw} \{ia_n A_{nm} \tilde{\mathbf{N}}_{nm}^{(3)} - b_n B_{nm} \tilde{\mathbf{M}}_{nm}^{(3)}\} \\ \mathbf{H}^{\text{sca}} = -H_0 \sum_{n=1}^{\infty} \sum_{m=-n}^n d_n^{pw} \{a_n A_{nm} \tilde{\mathbf{M}}_{nm}^{(3)} + ib_n B_{nm} \tilde{\mathbf{N}}_{nm}^{(3)}\} \end{cases}, \quad (5)$$

where (a_n, b_n) and (c_n, d_n) are the scattering coefficients obtained from the boundary conditions [24]. Similar to the BSCs, the scattering coefficients depend also on the time convention, which was not indicated in Ref. [25]. The far-field scattered light can be calculated with Eq. (5) in the limit of $\rho \rightarrow \infty$.

B. Formulations of BSCs in GLMT

We consider an EGB which is propagating along the positive z axis and whose center is located at (x_0, y_0, z_0) . In the negative time convention $\exp(-i\omega t)$, the beam field can be described by a scalar function [26,27]:

$$A(\mathbf{r}) = -i\sqrt{Q_x Q_y} e^{iQ_x \left(\frac{x-x_0}{w_{0x}}\right)^2 + iQ_y \left(\frac{y-y_0}{w_{0y}}\right)^2 + ik(z-z_0)}, \quad (6)$$

where w_{0x} and w_{0y} are the beam waist radii along the x and y axes. The corresponding beam confinement parameters are $s_x = 1/kw_{0x}$ and $s_y = 1/kw_{0y}$. The parameters Q_x and Q_y are defined as

$$\begin{cases} Q_x = [2s_x^2 k(z-z_0) - i]^{-1} \\ Q_y = [2s_y^2 k(z-z_0) - i]^{-1} \end{cases}. \quad (7)$$

When the electric field is x polarized in the plane of the beam waist (i.e., $z = z_0$), the radial field components of the EGB can be written as

$$\begin{cases} E_r^{\text{inc}} = E_0 \left(\frac{x}{r} - \frac{z}{ikr} \frac{\partial}{\partial x} \right) A(\mathbf{r}) \\ H_r^{\text{inc}} = H_0 \left(\frac{y}{r} - \frac{z}{ikr} \frac{\partial}{\partial y} \right) A(\mathbf{r}) \end{cases}. \quad (8)$$

In the quadrature method of GLMT, the BSCs A_{nm} and B_{nm} are expressed in two-dimensional integrations, one over the polar angle θ and the other over the azimuth angle ϕ :

$$\begin{aligned} \begin{pmatrix} A_{nm} \\ B_{nm} \end{pmatrix} &= \frac{(-i)^{n+1}}{\pi(2n+1)\psi_n(\rho)} \\ &\times \int_0^\pi d\theta \sin \theta \tilde{P}_n^m(\cos \theta) \int_0^{2\pi} d\phi e^{-im\phi} \begin{pmatrix} E_r^{\text{inc}}/E_0 \\ H_r^{\text{inc}}/H_0 \end{pmatrix}. \end{aligned} \quad (9)$$

Here, $\psi_n(\rho) = Z_n^{(1)}(\rho)$ is the first kind Riccati-Bessel function. Since the low-order corrected EGB description is only an approximate solution to Maxwell's equations, the BSCs show a dependence on the value of the radius ρ . Therefore, a specific value $\rho_n = n + 0.5$ is used in numerical computation [7]. This special value of the radius is the same as what is used in the original LA, and it can be regarded as the radial localization. The radial localization produces a remodeling of the beam in the quadrature method.

The following procedure of deduction is straightforward but very tedious. After some algebraic manipulation, we have the formulations of BSCs for the EGB [22]:

$$\begin{pmatrix} A_{nm} \\ B_{nm} \end{pmatrix} = \gamma_0 \int_0^\pi \gamma_1 \begin{pmatrix} \gamma_2^A \\ \gamma_2^B \end{pmatrix} d\theta, \quad (10)$$

where the factors γ_0 , γ_1 , and (γ_2^A, γ_2^B) are defined as

$$\gamma_0 = \frac{(-i)^n}{(2n+1)} \frac{\rho_n^2}{\psi_n(\rho_n)} e^{-ikz_0}, \quad (11)$$

$$\begin{aligned} \gamma_1 &= \sin \theta \tilde{P}_n^m(\cos \theta) \sqrt{Q_x Q_y} \\ &\times e^{\frac{i}{2}(Q_x s_x^2 + Q_y s_y^2) \rho_n^2 \sin^2 \theta + ik^2(Q_x s_x^2 x_0^2 + Q_y s_y^2 y_0^2) + i\rho \cos \theta}, \end{aligned} \quad (12)$$

$$\begin{cases} \gamma_2^A = \sin \theta (2Q_x s_x^2 \rho_n \cos \theta - 1) (I_{m-1}^\phi + I_{m+1}^\phi) \\ \quad - 4Q_x s_x^2 k x_0 \cos \theta \cdot I_m^\phi \\ \gamma_2^B = i \sin \theta (2Q_y s_y^2 \rho_n \cos \theta - 1) (I_{m+1}^\phi - I_{m-1}^\phi) \\ \quad - 4Q_y s_y^2 k y_0 \cos \theta \cdot I_m^\phi \end{cases}. \quad (13)$$

Here, I_m^ϕ represents the integration over the azimuth angle,

$$I_m^\phi = \frac{1}{2\pi} \int_0^{2\pi} e^{i\chi \cos(2\phi) + \gamma \cos(\phi-\xi) - im\phi} d\phi, \quad (14)$$

which can be further transformed into an infinite series of the modified Bessel functions (see Refs. [21,22]):

$$I_m^\phi = \sum_{s=-\infty}^{\infty} I_s(\chi) I_{m+2s}(\gamma) e^{-i(m+2s)\xi}. \quad (15)$$

The parameters χ , γ , and ξ are defined with

$$\chi = \frac{i}{2} \rho_n^2 \sin^2 \theta (Q_x s_x^2 - Q_y s_y^2), \quad (16)$$

$$\gamma = -i2\rho_n G_{xy} \sin \theta, \quad (17)$$

$$\begin{cases} G_{xy} = \sqrt{(Q_x s_x^2 k x_0)^2 + (Q_y s_y^2 k y_0)^2} \\ \cos \xi = Q_x s_x^2 k x_0 / G_{xy} \\ \sin \xi = Q_y s_y^2 k y_0 / G_{xy} \end{cases}. \quad (18)$$

In Eqs. (10)–(18), the radius is localized at $\rho_n = n + 0.5$. Combined with another localization of the polar angle at $\theta = \pi/2$, the formulation of BSCs can be further simplified to

$$\begin{pmatrix} A_{n,m} \\ iB_{n,m} \end{pmatrix} = -Z_n^m \tilde{\psi}_0^0 e^{-ikz_0} (\tilde{I}_{m-1}^\phi \pm \tilde{I}_{m+1}^\phi). \quad (19)$$

The pre-factor Z_n^m and the factor $\tilde{\psi}_0^0$ are given as [18]

$$Z_n^m = i^{1-|m|} (n+0.5)^{\frac{1}{2}-|m|} \sqrt{\frac{(n+|m|)!}{(n-|m|)!}}, \quad (20)$$

$$\tilde{\psi}_0^0 = -i\sqrt{\bar{Q}_x \bar{Q}_y} e^{\frac{i}{2}(\bar{Q}_x s_x^2 + \bar{Q}_y s_y^2) \rho_n^2 + ik^2(\bar{Q}_x s_x^2 x_0^2 + \bar{Q}_y s_y^2 y_0^2)}. \quad (21)$$

Here, the bar denotes that these parameters have been treated by the localizations (i.e., replace ρ and θ with $n + 0.5$ and $\pi/2$).

C. Formulations of BSCs in the ASD Method

The angular spectrum representation is a powerful technique to describe beam fields in homogeneous media. The beam field is described as a superposition of plane waves and evanescent waves, which are solutions to Maxwell's equations. Usually, the ASD is implemented by analyzing the angular spectrum of the vector potential of the beam [10] or the electromagnetic field itself [18]. In this work, we start from the scalar function

$A(\mathbf{r})$, which has been given in Eq. (6). The two-dimensional Fourier transform of $A(\mathbf{r})$ in the plane $z = 0$ that is perpendicular to the beam propagation direction is obtained as

$$\hat{A}(k_x, k_y; z = 0) = \pi w_{0x} w_{0y} e^{-\frac{1}{4}(k_x^2 w_{0x}^2 + k_y^2 w_{0y}^2)} e^{-i\mathbf{k} \cdot \mathbf{r}_0}. \quad (22)$$

Therefore, the Fourier spectra at an arbitrary plane $z = \text{constant}$ can be given by $\hat{A}(k_x, k_y; z) = \hat{A}(k_x, k_y; z = 0) e^{ik_z z}$ if $A(\mathbf{r})$ satisfies the Helmholtz equation $(\nabla^2 + k^2)A(\mathbf{r}) = 0$. The inverse Fourier transform of $\hat{A}(k_x, k_y; z)$ leads to the angular spectrum representation of the beam:

$$A(\mathbf{r}) = \frac{w_{0x} w_{0y}}{4\pi} \int_{-\infty}^{+\infty} \int_{-\infty}^{+\infty} e^{-\frac{1}{4}(k_x^2 w_{0x}^2 + k_y^2 w_{0y}^2)} e^{i\mathbf{k} \cdot (\mathbf{r} - \mathbf{r}_0)} dk_x dk_y, \quad (23)$$

in which there are two different types of plane waves. Within the region $k_x^2 + k_y^2 \leq k^2$, each plane wave is homogeneous and propagates in a direction, as illustrated in Fig. 1. However, within the complementary domain $k_x^2 + k_y^2 > k^2$, the plane wave is evanescent, propagates in a direction parallel to the xy plane, and decays exponentially with increasing z . For a loosely focused EGB, we have $kw_{0x} \gg 1$ and $kw_{0y} \gg 1$, and, hence, the exponential function $\exp[-(k_x^2 w_{0x}^2 + k_y^2 w_{0y}^2)/4]$ decays rapidly when $k_x^2 + k_y^2 \rightarrow k^2$. This indicates that the evanescent waves do not visibly contribute to the beam field. Therefore, the integration can be limited in the region $k_x^2 + k_y^2 \leq k^2$ [26].

The substitution of Eq. (23) into Eq. (8) leads to the angular spectrum representation of the radial component of the electric field:

$$E_r^{\text{inc}} = E_0 \frac{w_{0x} w_{0y}}{4\pi} \times \int_{-\infty}^{+\infty} \int_{-\infty}^{+\infty} \left(\frac{x}{r} - \frac{z}{r} \frac{k_x}{k} \right) e^{-\frac{1}{4}(k_x^2 w_{0x}^2 + k_y^2 w_{0y}^2)} e^{i\mathbf{k} \cdot (\mathbf{r} - \mathbf{r}_0)} dk_x dk_y. \quad (24)$$

Since $A(\mathbf{r})$ is only an approximate expression of the EGB, it does not strictly satisfy the Helmholtz equation $(\nabla^2 + k^2)A(\mathbf{r}) = 0$. Looking at Eq. (24), we may find that the first and second terms of the integrand are, respectively, the projections/contributions of E_x^{inc} and E_z^{inc} of the plane wave to the radial component of electric field E_r^{inc} . The vector $(1, 0, -k_x/k)$ represents the direction of the electric field, and (k_x, k_y, k_z) is the propagation direction of the plane wave. Nonetheless, the scalar product of $(1, 0, -k_x/k)$ and (k_x, k_y, k_z) is not equal to zero. This suggests that the remodeling must be given to the radial component E_r^{inc} , i.e., replacing $(1, 0, -k_x/k)$ with $(k_z/k, 0, -k_x/k)$.

In the spherical coordinate system, as illustrated in Fig. 1, we have $k_x = k \sin \alpha \cos \beta$ and $k_y = k \sin \alpha \sin \beta$, wherein α is the polar angle and β is the azimuth angle of the wave vector \mathbf{k} . By limiting the integration in the region $k_x^2 + k_y^2 \leq k^2$ and using the relation $dk_x dk_y = k^2 \sin \alpha \cos \alpha d\alpha d\beta$, Eq. (24) can be further developed to

$$E_r^{\text{inc}} = \frac{E_0}{4\pi s_x s_y} \int_0^{\pi/2} d\alpha \sin \alpha \cos \alpha e^{i\rho \cos \theta \cos \alpha} \times \int_0^{2\pi} d\beta (\sin \theta \cos \phi \cos \alpha - \cos \theta \sin \alpha \cos \beta) e^{-\frac{\sin^2 \alpha}{4} \left(\frac{\cos^2 \beta}{s_x^2} + \frac{\sin^2 \beta}{s_y^2} \right)} e^{i\rho \sin \theta \sin \alpha \cos(\phi - \beta)} e^{-i\mathbf{k} \cdot \mathbf{r}_0}. \quad (25)$$

In the next step, we substitute Eq. (25) into Eq. (9) and then interchange the order of integrals over (θ, ϕ) and (α, β) , leading to

$$A_{nm} = \frac{(-i)^{n+1}}{4\pi^2 s_x s_y (2n+1) \psi_n(\rho)} \int_0^{\pi/2} d\alpha \sin \alpha \cos \alpha \int_0^{2\pi} d\beta e^{-\frac{\sin^2 \alpha}{4} \left(\frac{\cos^2 \beta}{s_x^2} + \frac{\sin^2 \beta}{s_y^2} \right)} e^{-i\mathbf{k} \cdot \mathbf{r}_0} \times \int_0^\pi d\theta \sin \theta \tilde{P}_n^m(\cos \theta) e^{i\rho \cos \alpha \cos \theta} \left\{ \frac{\sin \theta \cos \alpha}{2} \left[\int_0^{2\pi} d\phi e^{i\rho \sin \alpha \sin \theta \cos(\phi - \beta) - i(m-1)\phi} + \int_0^{2\pi} d\phi e^{i\rho \sin \alpha \sin \theta \cos(\phi - \beta) - i(m+1)\phi} \right] \right. \\ \left. - \cos \theta \sin \alpha \cos \beta \int_0^{2\pi} d\phi e^{i\rho \sin \alpha \sin \theta \cos(\phi - \beta) - im\phi} \right\}. \quad (26)$$

The ϕ integration in Eq. (26) can be transformed into Bessel functions:

$$A_{nm} = \frac{-i^{m-n}}{2\pi s_x s_y (2n+1) \psi_n(\rho)} \int_0^{\pi/2} d\alpha \sin \alpha \cos \alpha \int_0^{2\pi} d\beta e^{-\frac{\sin^2 \alpha}{4} \left(\frac{\cos^2 \beta}{s_x^2} + \frac{\sin^2 \beta}{s_y^2} \right)} e^{-i\mathbf{k} \cdot \mathbf{r}_0} e^{-im\beta} \times \int_0^\pi d\theta \sin \theta \tilde{P}_n^m(\cos \theta) e^{i\rho \cos \alpha \cos \theta} \left\{ i \sin \beta \frac{\cos \alpha}{\rho \sin \alpha} m J_m(\rho \sin \alpha \sin \theta) + \right. \\ \left. \cos \beta [\sin \theta \cos \alpha J'_m(\rho \sin \alpha \sin \theta) - i \cos \theta \sin \alpha J_m(\rho \sin \alpha \sin \theta)] \right\}. \quad (27)$$

Substituting the identity of Eq. (28) [28] and its derivative of α [i.e., Eq. (29)] into Eq. (27),

$$\int_0^\pi d\theta \sin \theta \tilde{P}_n^m(\cos \theta) J_m(\rho \sin \alpha \sin \theta) e^{i\rho \cos \alpha \cos \theta} = 2i^{m-n} j_n(\rho) \tilde{P}_n^m(\cos \alpha). \quad (28)$$

$$\int_0^\pi d\theta \sin \theta \tilde{P}_n^m(\cos \theta) \left\{ \cos \alpha \sin \theta J'_m(\rho \sin \alpha \sin \theta) - i \sin \alpha \cos \theta J_m(\rho \sin \alpha \sin \theta) \right\} e^{i\rho \cos \alpha \cos \theta} = 2i^{n-m} j_n(\rho) \frac{d\tilde{P}_n^m(\cos \alpha)}{d\alpha}. \quad (29)$$

Thus, the non-radial dependence of the BSCs is achieved, which benefits from the remodeling in Eq. (25). Replacing the factor $e^{-ik \cdot \mathbf{r}_0}$ with spherical coordinates, we have

$$A_{nm} = \frac{-i^{1-m}}{(2n+1)s_x s_y} \int_0^{\pi/2} d\alpha \sin \alpha \cos \alpha e^{-\frac{\sin^2 \alpha}{8}(s_x^2 + s_y^2)} e^{-ikz_0 \cos \alpha} \times \left\{ [\cos \alpha \cdot m\tilde{\pi}_n^m(\alpha) + \tilde{\tau}_n^m(\alpha)]X_{m-1}(\alpha) + [\cos \alpha \cdot m\tilde{\pi}_n^m(\alpha) - \tilde{\tau}_n^m(\alpha)]X_{m+1}(\alpha) \right\}. \quad (30)$$

The β -dependent terms are separated from the functions to be integrated, and the β integration $X_m(\alpha)$ is given as

$$X_m(\alpha) = \frac{i^m}{2\pi} \int_0^{2\pi} e^{\chi \cos 2\beta - i\gamma \cos(\beta - \xi_0) - im\beta} d\beta. \quad (31)$$

The parameters used in Eqs. (30) and (31) are defined as

$$\chi = (s_y^{-2} - s_x^{-2}) \sin^2 \alpha / 8, \quad (32)$$

$$\gamma = \rho_0 \sin \alpha, \quad (33)$$

$$\begin{cases} \rho_0 = k\sqrt{x_0^2 + y_0^2} \\ \cos \xi_0 = kx_0 / \rho_0 \\ \sin \xi_0 = ky_0 / \rho_0 \end{cases} \quad (34)$$

The β integration of Eq. (31) is very similar to that of Eq. (14), so we can follow the same procedure given in Ref. [21]. Finally, it is transformed into a series of (modified) Bessel functions:

$$X_m(\alpha) = \sum_{s=-\infty}^{\infty} (-1)^s I_s(\chi) J_{m+2s}(\gamma) e^{-i(m+2s)\xi_0}. \quad (35)$$

By repeating the same procedure of deduction on the radial component of magnetic field H_r , the formulation of B_{nm} can be obtained.

As the result, the BSCs of the EGB in the ASD method are expressed as below:

$$\begin{pmatrix} A_{nm} \\ iB_{nm} \end{pmatrix} = \frac{-i^{1-m}}{(2n+1)s_x s_y} \int_0^{\pi/2} d\alpha \sin \alpha \cos \alpha e^{-\frac{\sin^2 \alpha}{8}(s_x^2 + s_y^2)} e^{-ikz_0 \cos \alpha} \times \left\{ \begin{aligned} & [\cos \alpha \cdot m\tilde{\pi}_n^m(\alpha) + \tilde{\tau}_n^m(\alpha)]X_{m-1}(\alpha) \\ & \pm [\cos \alpha \cdot m\tilde{\pi}_n^m(\alpha) - \tilde{\tau}_n^m(\alpha)]X_{m+1}(\alpha) \end{aligned} \right\}. \quad (36)$$

The CGB is a special case of the EGB when $w_{0x} = w_{0y} = w_0$. In this case, the parameter χ defined in Eqs. (16) and (32) is equal to zero. Therefore, the function I_m^ϕ described in Eq. (15) can be simplified to

$$I_m^\phi = I_m(\gamma) e^{-im\xi}, \quad (37)$$

and the function $X_m(\alpha)$ of Eq. (35) is simplified to

$$X_m(\alpha) = J_m(\gamma) e^{-im\xi_0}. \quad (38)$$

This leads to the same expressions of BSCs of Ref. [18].

3. NUMERICAL RESULTS AND DISCUSSION

A. General Description of Numerical Computation

Numerical computation of the BSCs involves the calculations of the NALFs \tilde{P}_n^m , the GLFs $\tilde{\pi}_n^m$ and $\tilde{\tau}_n^m$, and the (modified) Bessel functions I_m and J_m . All of these functions can be computed by using their recurrence relations, which have been

extensively discussed in the literature. The use of the normalization factor of the associated Legendre function can limit the values of the relevant functions (i.e., \tilde{P}_n^m , $\tilde{\pi}_n^m$, and $\tilde{\tau}_n^m$) within reasonable ranges. In our case, attention should be paid to the numerical computation of the modified Bessel function I_m , because the value of the function increases rapidly when the real part of its argument increases, and it may exceed the limit of the floating number. This can be avoided by using the method introduced in Ref. [21].

The calculation of the infinite series of (modified) Bessel functions is required in the LA method, the quadrature and ASD methods using one-dimensional integration [see Eqs. (15) and (35)]. Summation of the series can be truncated, depending on the involved parameters (i.e., γ , χ , and ξ_0) and the azimuth index m . The criterion for the range of the integer s can be easily evaluated because the (modified) Bessel function decreases very fast when the order is high enough.

Numerical computation of the BSCs with the quadrature and ASD methods involves the integrations of violently oscillatory functions. In order to improve the accuracy and the efficiency of the BSC calculation, the numerical integration is performed by subdividing the interval into several equidistant ones. For each subinterval, the Romberg method combined with the composite trapezoidal rule is employed.

The task of BSC calculation for given beam parameters is decided as follows: (1) the partial wave order is truncated at n_t when $\max\{|A_{n,m}|, |B_{n,m}|\} < 10^{-10}$ is satisfied for a fixed low azimuth mode $m = 1$; (2) for a certain partial wave n , the azimuth index is truncated at m_t when $\max\{|A_{n,m}|, |B_{n,m}|\} < 10^{-10} \max\{|A_{n,1}|, |B_{n,1}|\}$ is met, otherwise $m_t = n$.

The BSC results are examined by reconstructing the beam field and comparing the constructed field with the given one. Afterwards, these BSCs that are validated are used for further calculations, such as the internal field and the near-/far-field scattering.

All of the numerical calculations discussed in the following sections are executed using the double-precision VC++6.0 codes on a personal computer powered by a 3.2 GHz CPU.

B. Efficiency of Numerical Computation

The BSCs of the EGB can be calculated alternatively with the quadrature method [i.e., Eqs. (10)–(18)], the LA method [i.e., Eqs. (19)–(21)], and the ASD method [i.e., Eqs. (31)–(36)]. The quadrature method and the ASD method can be implemented with one- or two-dimensional integrations, depending on the way to calculate the azimuth-dependent functions (i.e., I_m^ϕ in the quadrature method and $X_m(\alpha)$ in the ASD method). A comparison of the CPU time for calculating the $X_m(\alpha)$ can be used to show the efficiency of the ASD method. Assuming the parameters $\lambda = 0.6328 \mu\text{m}$, $w_{0x} = 3w_{0y} = 6 \mu\text{m}$, $\xi_0 = \pi/4$, and $\alpha = 0.3 \text{ rad}$, we calculate $X_m(\alpha)$ for $m = 1$ with Eq. (35). It costs about 0.17 s for ten thousand repeats. The same calculation using the integral of Eq. (31) with a desired accuracy of 1×10^{-5} requires about 3.16 s. For the calculation of $X_m(\alpha)$ for $m = 20$, the CPU times required in these calculations are 0.16 s and 6.11 s, respectively. This indicates

that the ASD method using the one-dimensional integration is at least ten times faster than the two-dimensional integrations. Such is also the case for the quadrature method.

A comparison of the efficiency between the ASD, quadrature, and LA methods can be made with the same beam parameters, e.g., $w_{0y} = 2w_{0x} = 5 \mu\text{m}$, $\lambda = 0.6328 \mu\text{m}$, $x_0 = 6 \mu\text{m}$, $y_0 = 4 \mu\text{m}$, and $z_0 = 0$. The CPU time of the ASD method using one-dimensional integration for evaluating all of the BSCs is about 1.66 h, the one-dimensional quadrature method requires about 20 h, and the LA method needs only 9.2 s. Among these methods, the LA is the most efficient, and the quadrature technique is the most time consuming. The ASD method is about ten times faster than the quadrature method. This is because the integrand in the quadrature method oscillates more violently and distributes more widely than that of the ASD method, as shown in Fig. 2. Further numerical study indicates that the CPU time required for evaluating all of the BSCs depends on both the beam waist radii (w_{0x} , w_{0y}) and the coordinates of the beam center (x_0 , y_0 , z_0). Notably, more CPU time is required when the beam center is far away from the z axis and when the beam ellipticity is high.

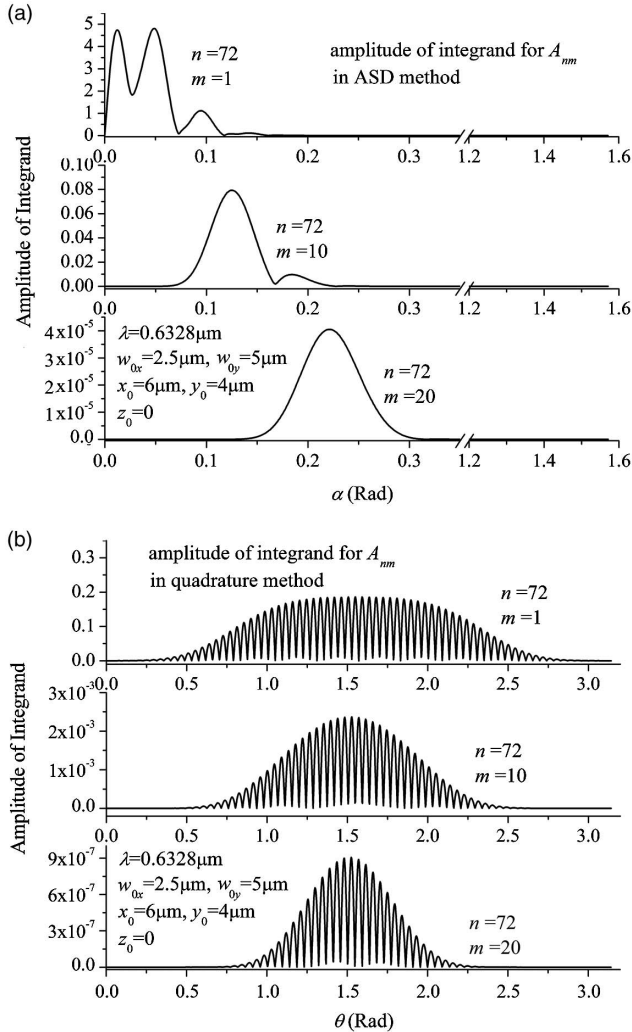


Fig. 2. Comparison of the integrands used in (a) the ASD method and (b) the quadrature method, wherein the partial wave order is $n = 72$ and the azimuth indices are $m = 1, 10$, and 20 , respectively.

C. Beam Reconstruction

As long as the BSCs have been calculated, the incident beam field can be reconstructed by using Eq. (3). A comparison between the reconstructed beam field and the given one can be used to validate the numerical method for evaluating the BSCs. An example of the reconstructed beam field is shown in Fig. 3 together with the beam parameters. The amplitude of the field at the beam center is assumed to be $E_0 = 1$. The field can be reconstructed in the region where $E > 10^{-8}$. Outside of this region, the reconstructed field is dominated by round-off

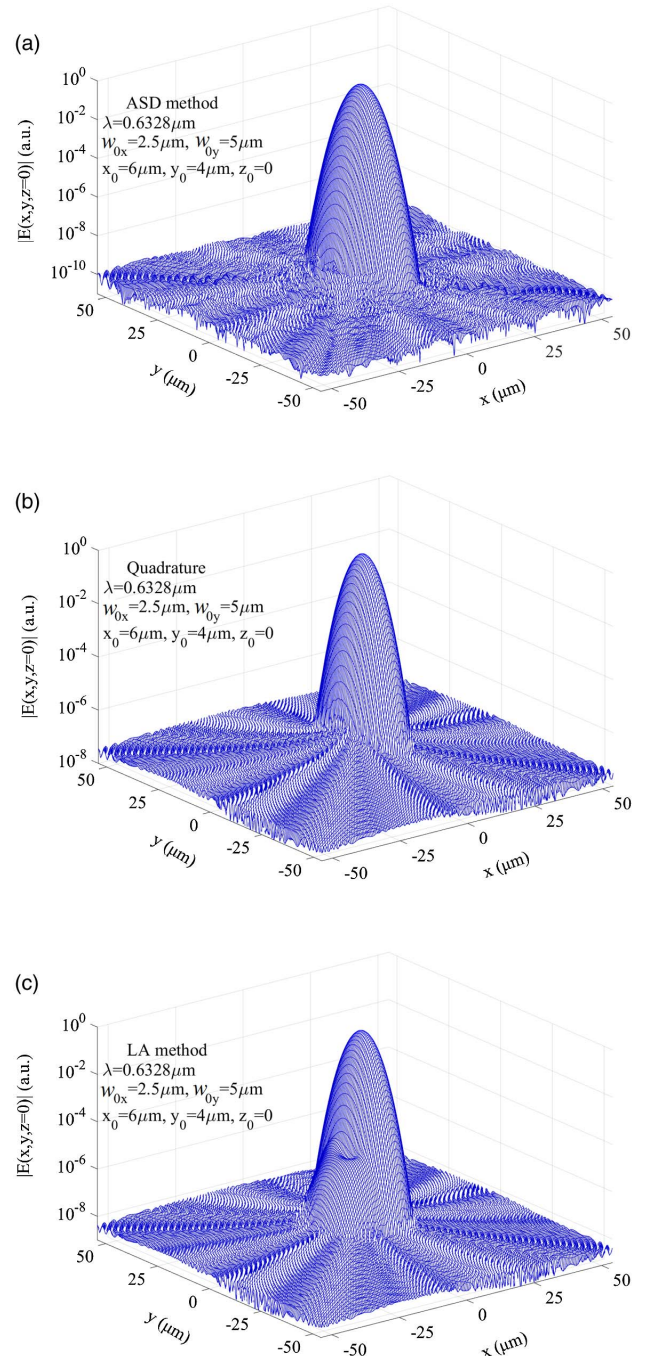


Fig. 3. Beam fields reconstructed by (a) the ASD method, (b) the quadrature method, and (c) the LA method.

errors, which is decided by the BSC results. The fidelity of the beam fields reconstructed by the ASD and quadrature methods to the given one is excellent. This implies that, although the remodeling in the ASD method is slightly different from that of quadrature method, both methods provide very nice approximations to the given field. The LA method can also reconstruct the intended peak satisfyingly, but it produces a pseudo-peak, whose level is about 1×10^{-6} [18,21,29]. The pseudo-peak is a result of the polar angle localization.

Further numerical study concerns the BSC calculation and the beam reconstruction for various locations and ellipticities of the beam. It is found that the ASD method is capable of

reconstructing the beam fields with high beam ellipticities and far off-axis locations. However, the beam fields reconstructed by the LA and quadrature methods are of poor quality for the far off-axis location (as shown in Fig. 4) and high beam ellipticity (Fig. 5). It can be seen that the ASD method can reproduce the beam field in the region where the level of the field is as low as 1×10^{-9} , while the LA and quadrature methods are limited at the level of about 1×10^{-3} . For more information, please refer to Ref. [22].

The superiority of the ASD method to the quadrature and LA methods can be attributed to its way for calculating the BSCs. As described in Eq. (36), the integrand of the ASD method includes a function $\exp[-\sin^2 \alpha(s_x^2 + s_y^2)/8]$, which distributes mainly in a narrow range of polar angles very close to zero. Therefore, the integration can be implemented within a narrow interval of small polar angles, in which it is not difficult to calculate the function $X_m(\alpha)$ accurately. Although the integrand of the quadrature method [see Eqs. (10)–(13)] includes functions similar to those of the ASD, the integrand of the quadrature method distributes much more widely, covering a range centered at $\pi/2$. The integrand cannot be calculated accurately for high partial waves of the EGB, because the I_m^ϕ calculation involves a delicate cancellation, and there can be a catastrophic loss of significance in the vicinity of $\theta = \pi/2$ [22]. This occurs for high beam ellipticity and far off-axis

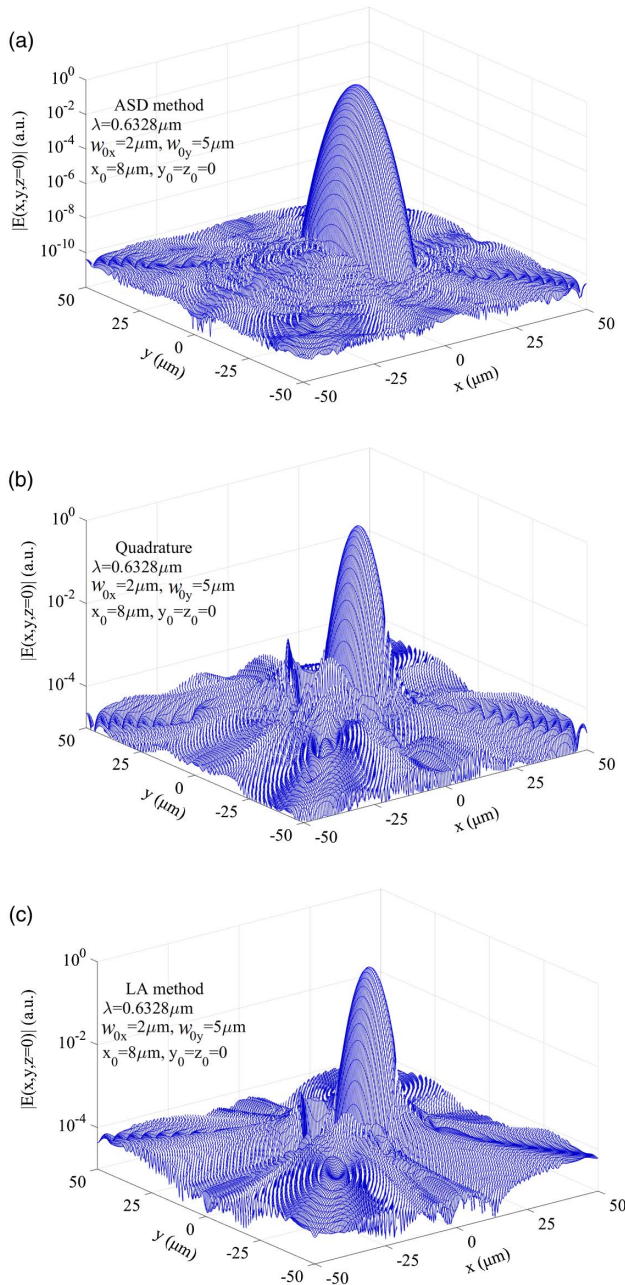


Fig. 4. Comparison of the reconstructed beam fields for far off-axis location. The parameters are $\lambda = 0.6328 \mu\text{m}$, $w_{0x} = 2 \mu\text{m}$, $w_{0y} = 5 \mu\text{m}$, $x_0 = 8 \mu\text{m}$, and $y_0 = z_0 = 0$.

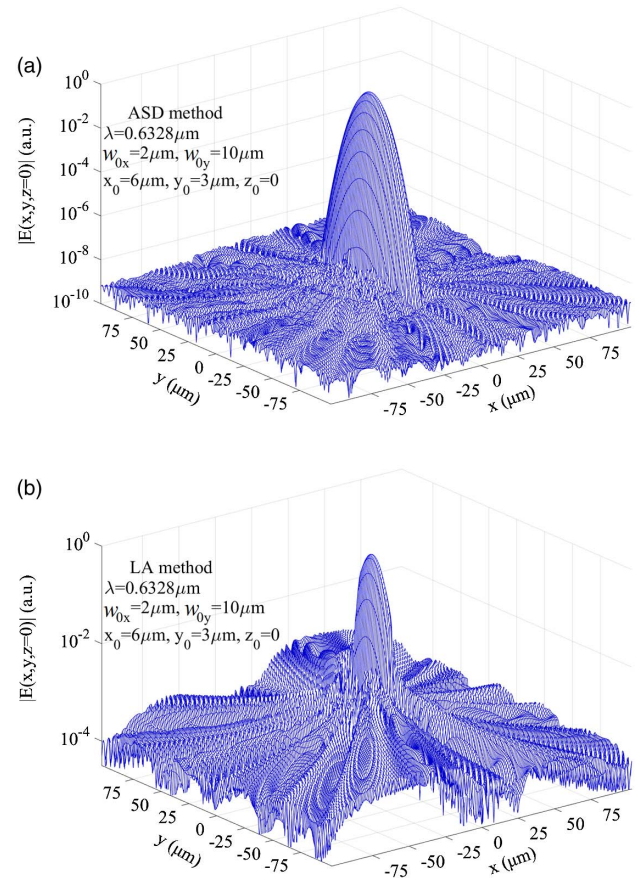


Fig. 5. Beam fields reconstructed by (a) the ASD method and (b) LA method. The parameters are $\lambda = 0.6328 \mu\text{m}$, $w_{0x} = 2 \mu\text{m}$, $w_{0y} = 10 \mu\text{m}$, $x_0 = 6 \mu\text{m}$, $y_0 = 3 \mu\text{m}$, and $z_0 = 0$.

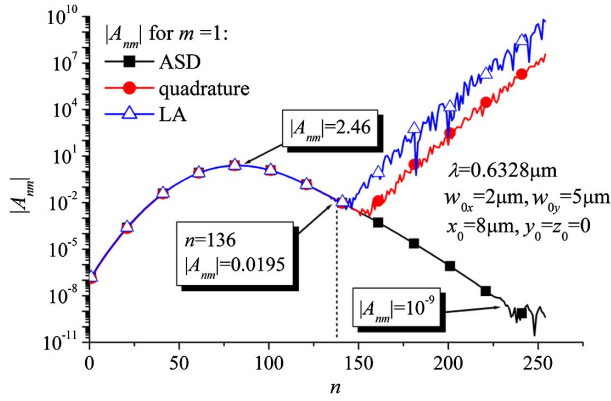


Fig. 6. Comparison of the BSCs evaluated by the ASD, the quadrature, and the LA methods. The parameters are the same as those in Fig. 4.

locations. The situation for the LA method can be even more serious because the localization is made at $\pi/2$. As an example, Fig. 6 shows a comparison of the BSCs calculated with these two methods, wherein the parameters are the same as those used in Fig. 4. It can be seen that the quadrature and LA methods acquire incorrect results of BSCs for partial waves $n > 136$. The extraordinary increase of the BSCs calculated by the LA method is caused by a complete loss of significant digits in the \tilde{I}_m^ϕ calculation [see Eq. (19)]. In the quadrature method, large errors are introduced in the calculation of the function I_m^ϕ in the vicinity of the polar angle $\pi/2$ [22]. It should be mentioned that the integral method for calculating the function I_m^ϕ , given in Eq. (14), does not improve the situation. The integration is in principle a sum of the functions in the interval, and, if the result of integration is much less than the maximum of the integrand, the significant digits are inevitably lost.

The incorrect BSCs may produce very strong ghost distributions in the reconstructed beam field. For example, those BSCs of $n > 136$ obtained in the quadrature and LA methods would affect the reconstructed beam field mainly in the region $r > 13.7 \mu\text{m}$. Therefore, in the beam reconstruction shown in Figs. 4 and 5, the partial waves are truncated at $n_t = 136$ in the quadrature and LA methods. The lack of sufficient BSCs limits the reliable beam reconstruction in a very narrow region.

D. Numerical Results of Light Scattering

The internal and the scattered fields can be calculated with Eqs. (4) and (5) using the BSCs of the incident beam and the scattering coefficients of the spherical particle. The far-field scattered light can be calculated with Eq. (5) in the limit of $\rho \rightarrow \infty$. The total field outside the particle includes both the incident and the scattered fields, i.e., $\mathbf{E}^{\text{ext}} = \mathbf{E}^{\text{inc}} + \mathbf{E}^{\text{sca}}$. Since the calculation of the Mie coefficients is well issued for the spherical particle [24,30], results of the internal and external fields depend mostly on the BSC calculation. Therefore, the BSCs can be validated by comparing the reconstructed beam field with the given field [22,29]. Alternatively, this can be done by comparing the scattered light with simulated results [11,31].

An example of far-field scattering in the xz plane is shown in Fig. 7, in which the beam parameters are the same as those used

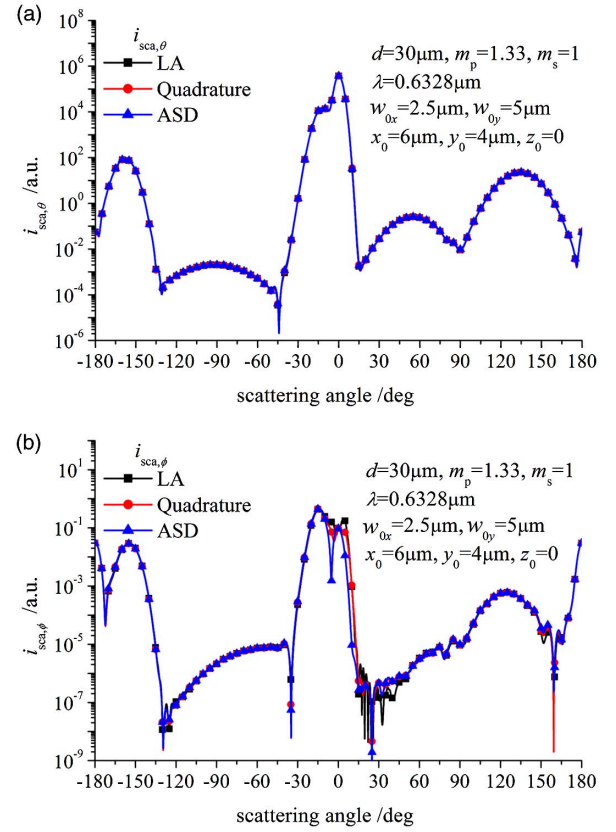


Fig. 7. Intensities of far-field scattering: (a) component polarized in the xz plane; (b) component perpendicular to the xz plane. The beam parameters are the same as those in Fig. 3. The particle diameter is $d = 30 \mu\text{m}$, and the refractive indices of the particle and the surrounding are $m_p = 1.33$ and $m_s = 1$.

in Fig. 3. The particle diameter is $d = 30 \mu\text{m}$, and the refractive indices of the particle and its surrounding medium are $m_p = 1.33$ and $m_s = 1$ (the relative refractive index is $\hat{m} = m_p/m_s = 1.33$). The scattered light intensities $i_{\text{sca},\theta}$ and $i_{\text{sca},\phi}$ are the components polarized in the scattering plane and perpendicular to the plane, respectively. The polar angle $\theta > 0$ represents the direction along the positive x axis and $\theta < 0$ the negative x axis. The component $i_{\text{sca},\phi}$ is about six orders weaker than $i_{\text{sca},\theta}$, indicating the destructive and constructive contributions of the partial waves, respectively. The components $i_{\text{sca},\theta}$ calculated with different methods agree with each other, due to the successful calculation of BSCs and the constructive interference of partial waves. Since the component $i_{\text{sca},\phi}$ is the destructive contribution of partial waves, the different remodeling effect of the methods is asserted in $i_{\text{sca},\phi}$.

Figure 8 gives another example of far-field scattering in the xz plane. The beam parameters are the same as those used in Fig. 5. Apparent differences can be found in both the parallel and perpendicular components $i_{\text{sca},\theta}$ and $i_{\text{sca},\phi}$ that are calculated with the LA and the ASD methods. It can be seen in Fig. 5 that the incident beam field reconstructed by the ASD method agrees with the given field much better than that of the LA method. Therefore, the results of scattered light calculated using the ASD method is more reliable. This suggests that, in order to get reliable results, the quality of beam

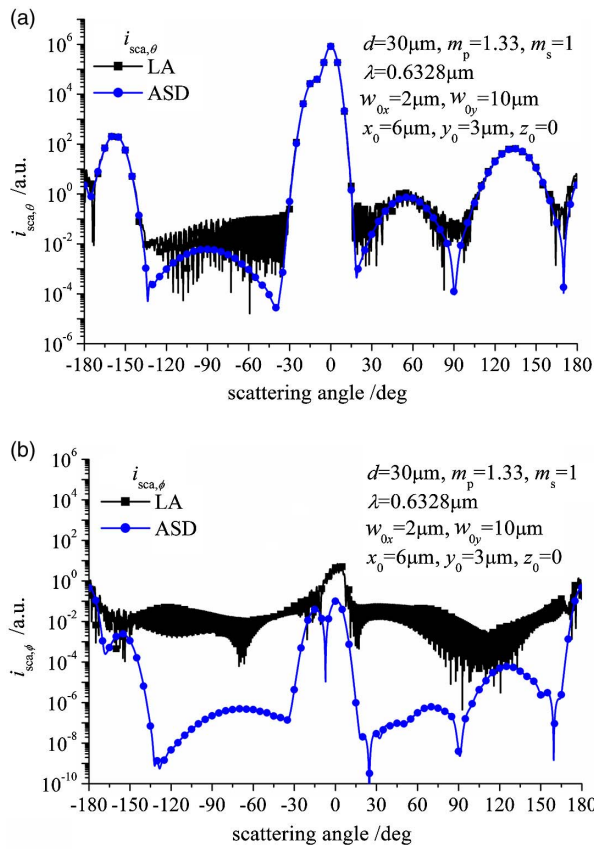


Fig. 8. Intensities of far-field scattering: (a) component polarized in the xz plane; (b) component perpendicular to the xz plane. The beam parameters are the same as those in Fig. 5. The particle diameter is $d = 30 \mu\text{m}$, and the refractive indices of the particle and the surrounding are $m_p = 1.33$ and $m_s = 1$.

reconstruction should be checked carefully before the BSCs are used for further calculation of light scattering.

Figure 9(a) shows the internal and near-surface fields in the xz plane (i.e., $y = 0 \mu\text{m}$) using the BSCs calculated with the ASD method. The beam parameters are the same as those described in Fig. 4(a), and the BSCs have been validated by checking the quality of the reconstructed field. The particle diameter is $d = 30 \mu\text{m}$, and the relative refractive index of the particle is $\hat{m} = 1.333$. Since the beam waist radii and the particle diameter are much bigger than the wavelength, and the beam waist in the x axis is much narrower than the particle diameter, the beam propagation can be explained with ray optics or Debye series [32]. As illustrated in the figure, $p = 0$ represents the reflection of the incident beam by the surface of the sphere, $p = 1$ and $p = 2$ are the refracted components, which undergo $p - 1$ internal reflections. Figure 9(b) shows the fields simulated with the Lumerical finite-difference time-domain (FDTD) solutions. A cubic domain $40 \mu\text{m} \times 40 \mu\text{m} \times 40 \mu\text{m}$ is selected, and the spherical particle is located at the center of the cube. The grid is terminated by the perfectly matched layer absorbing boundary condition. The simulated result becomes very similar to the numerical result of Fig. 9(a), when the discretization step is as low as $0.05 \mu\text{m}$ (i.e., about $\lambda/13$) in each direction.

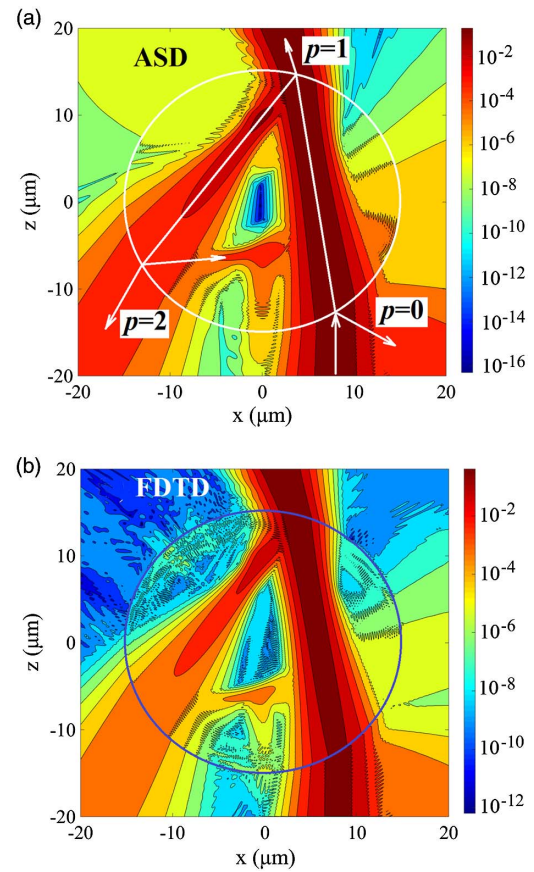


Fig. 9. Internal and near-surface fields in the xz plane ($y = 0 \mu\text{m}$). The spherical particle is illuminated by an EGB, whose parameters are the same as those of Fig. 4. The particle diameter is $d = 30 \mu\text{m}$, and the relative refractive index is $\hat{m} = 1.333$. (a) Result of ASD method and (b) result simulated with the FDTD method.

Figure 10 shows the external field in the xy plane of $z = 100 \mu\text{m}$. The beam waist radii are $w_{0x} = 10 \mu\text{m}$ and $w_{0y} = 20 \mu\text{m}$. The particle diameter is $d = 10 \mu\text{m}$, and the relative refractive index is $\hat{m} = 1.333$. The beam center is located at $x_0 = 3 \mu\text{m}$, $y_0 = 5 \mu\text{m}$, and $z_0 = -300 \mu\text{m}$. In this case, the distance between the beam center and the

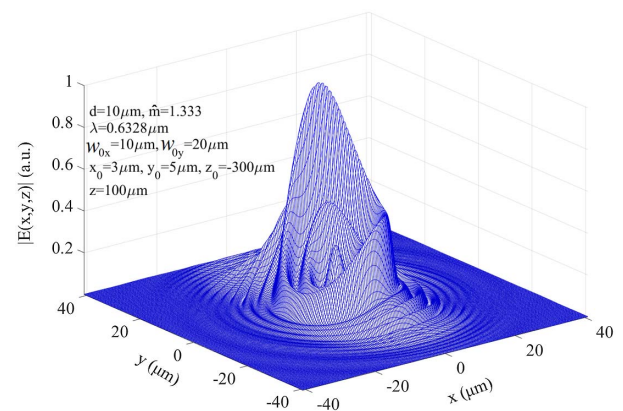


Fig. 10. Near-surface field in the xy plane ($z = 100 \mu\text{m}$). The spherical particle is illuminated by an EGB. All of the parameters are illustrated in the figure.

z axis is $5.83\ \mu\text{m}$, which is much less than w_{0x} and w_{0y} . The ellipticity of the beam cross-section is not high. Therefore, all of the methods (i.e., the LA, the quadrature, and the ASD methods) can achieve reliable results of BSCs, leading to reliable results of the external fields.

4. CONCLUSION

Formulations of the BSCs for an EGB are derived by using the angular spectra representation of the radial components of the beam field. Such a deduction reveals the difference of beam remodeling made in the quadrature, the LA, and the ASD methods.

In both the quadrature and ASD methods for BSC calculation, the integration over n azimuth angle can be transformed into the infinite series of (modified) Bessel functions, which can greatly speed up the numerical computation. Numerical study shows that the one-dimensional integration of the ASD method is at least ten times faster than the two-dimensional integrations, and it is ten times faster than the quadrature method, because the functions to be integrated are not as seriously oscillatory as those in the quadrature method.

The calculated BSCs are used for reconstructing the beam field. The fidelity of the reproduced field to the given one can be used to examine the BSC calculation. It is found that, when the beam center is very close to the z axis, and the beam ellipticity is not very high, both the quadrature and LA methods can evaluate the BSCs of the EGB accurately. But, when the EGB is located far off-axis and/or the beam ellipticity is high, incorrect values of BSCs are obtained. The ASD method, however, can acquire reliable results and reconstruct the beam field satisfactorily in the region where $E > 10^{-8}$. The ability of the ASD method to evaluate the BSCs is insensitive to the beam ellipticity and the beam location. Numerical study on this issue reveals that the difficulty in the quadrature and LA methods is caused by the loss of significant digits in the calculation of azimuth-dependent functions, which does not occur in the ASD method. Therefore, it can be concluded that the ASD method is more powerful and reliable for evaluating the BSCs of the EGB than the other two methods. The calculation of internal and external fields depends mainly on the BSCs. In this work, the BSCs are validated mainly by checking the quality of the reconstructed incident beam field so as to get reliable results of light scattering.

Funding. National Natural Science Foundation of China (NSFC) (51476104, 51506129).

Acknowledgment. The authors express their gratitude to Dr. Geng Tao for his help simulating the scattered field on the FDTD method.

REFERENCES

- W. Zeng, M. Xu, Y. Zhang, and Z. Wang, "Laser sheet drop sizing of evaporating sprays using simultaneous LIEF/MIE techniques," *Proc. Combust. Inst.* **34**, 1677–1685 (2013).
- A. A. Naqwi, X. Liu, and F. Durst, "Evaluation of the dual-cylindrical wave laser technique for sizing of liquid droplets," *Part. Part. Syst. Charact.* **9**, 44–51 (1992).
- V. Garcés-Chávez, D. McGloin, H. Melville, W. Sibbett, and K. Dholakia, "Simultaneous micromanipulation in multiple planes using a self-reconstructing light beam," *Nature* **419**, 145–147 (2002).
- D. Grier, "A revolution in optical manipulation," *Nature* **424**, 810–816 (2003).
- Y. J. Yuan, K. F. Ren, S. Coëtmelec, and D. Lebrun, "Rigorous description of holograms of particles illuminated by an astigmatic elliptical Gaussian beam," *J. Phys. Conf. Ser.* **147**, 012052 (2009).
- N. Verrier, S. Coëtmelec, M. Brunel, D. Lebrun, and A. Janssen, "Digital in-line holography with an elliptical, astigmatic Gaussian beam: wide-angle reconstruction," *J. Opt. Soc. Am. A* **25**, 1459–1466 (2008).
- G. Gouesbet and G. Gréhan, *Generalized Lorenz-Mie Theories* (Springer, 2011).
- W. L. Moreira, A. A. R. Neves, M. K. Garbos, T. G. Euser, and C. L. Cesar, "Expansion of arbitrary electromagnetic fields in terms of vector spherical wave functions," *Opt. Express* **24**, 2370–2382 (2016).
- P. C. Clemmow, "Plane wave representation," in *The Plane Wave Spectrum Representation of Electromagnetic Fields* (Pergamon, 1966), pp. 11–38.
- A. Doicu and T. Wriedt, "Plane wave spectrum of electromagnetic beams," *Opt. Commun.* **136**, 114–124 (1997).
- D. P. Chrissoulidis and E. Richalot, "Wave-amplitude synthesis applied to Gaussian-beam scattering by an off-axis sphere," *J. Opt. Soc. Am. A* **34**, 558–567 (2017).
- G. Gouesbet, C. Letellier, K. F. Ren, and G. Gréhan, "Discussion of two quadrature methods of evaluating beam-shape coefficients in generalized Lorenz-Mie theory," *Appl. Opt.* **35**, 1537–1542 (1996).
- G. Gouesbet, G. Gréhan, and B. Maheu, "Expressions to compute the coefficients g_n^m in the generalized Lorenz-Mie theory using finite series," *J. Opt.* **19**, 35–48 (1988).
- G. Gouesbet, G. Gréhan, and B. Maheu, "On the generalized Lorenz-Mie theory: first attempt to design a localized approximation to the computation of the coefficients g_n^m ," *J. Opt.* **20**, 31–43 (1989).
- G. Gouesbet, G. Gréhan, and B. Maheu, "Localized interpretation to compute all the coefficients g_n^m in the generalized Lorenz-Mie theory," *J. Opt. Soc. Am. A* **7**, 998–1007 (1990).
- K. F. Ren, G. Gouesbet, and G. Gréhan, "Integral localized approximation in generalized Lorenz-Mie theory," *Appl. Opt.* **37**, 4218–4225 (1998).
- H. C. van de Hulst, *Light Scattering by Small Particles* (Wiley, 1957).
- J. Qiu and J. Shen, "Beam shape coefficient calculation for a Gaussian beam: localized approximation, quadrature and angular spectrum decomposition methods," *Appl. Opt.* **57**, 302–313 (2018).
- K. F. Ren, G. Gréhan, and G. Gouesbet, "Laser sheet scattering by spherical particles," *Part. Part. Syst. Charact.* **10**, 146–151 (1993).
- G. Gréhan, K. F. Ren, G. Gouesbet, A. Naqwi, and F. Durst, "Evaluation of a particle sizing technique based on laser sheets," *Part. Part. Syst. Charact.* **11**, 101–106 (1994).
- J. Shen, X. Jia, and H. Yu, "Compact formulation of the beam shape coefficients for elliptical Gaussian beam based on localized approximation," *J. Opt. Soc. Am. A* **33**, 2256–2263 (2016).
- W. Wang and J. Shen, "Beam shape coefficients calculation for an elliptical Gaussian beam with 1-dimensional quadrature and localized approximation methods," *J. Quant. Spectrosc. Radiat. Transfer* **212**, 139–148 (2018).
- J. P. Barton, D. R. Alexander, and S. A. Schaub, "Internal and near-surface electromagnetic fields for a spherical particle irradiated by a focused laser beam," *J. Appl. Phys.* **64**, 1632–1639 (1988).
- C. F. Bohren and D. R. Huffman, *Absorption and Scattering of Light by Small Particles* (Wiley, 1983).
- J. J. Wang and G. Gouesbet, "Note on the use of localized beam models for light scattering theories in spherical coordinates," *Appl. Opt.* **51**, 3832–3836 (2012).
- W. H. Carter, "Electromagnetic field of a Gaussian beam with an elliptical cross section," *J. Opt. Soc. Am.* **62**, 1195–1201 (1972).
- K. F. Ren, G. Gréhan, and G. Gouesbet, "Electromagnetic field expression of a laser sheet and the order of approximation," *J. Opt.* **25**, 165–176 (1994).
- A. A. R. Neves, L. A. Padilha, A. Fontes, E. Rodriguez, C. H. B. Cruz, L. C. Barbosa, and C. L. Cesar, "Analytical results for a Bessel

- function times Legendre polynomials class integrals," *J. Phys. A* **39**, L293–L296 (2006).
29. G. Gouesbet and J. A. Lock, "Rigorous justification of the localized approximation to the beam-shape coefficients in generalized Lorenz–Mie theory. II. Off-axis beams," *J. Opt. Soc. Am. A* **11**, 2516–2525 (1994).
30. L. Liu, H. Wang, B. Yu, Y. Xu, and J. Shen, "Improved algorithm of light scattering by a coated sphere," *China Particuol.* **5**, 230–236 (2007).
31. F. Frezze, F. Mangini, and N. Tedeschi, "Introduction to electromagnetic scattering: tutorial," *J. Opt. Soc. Am. A* **35**, 163–173 (2018).
32. S. Qin, R. Li, R. Yang, and C. Ding, "Debye series analysis of internal and near-surface fields for a homogeneous sphere illuminated by an axicon-generated vector Bessel beam," *J. Quant. Spectrosc. Radiat. Transfer* **195**, 26–34 (2017).